ORIGINAL PAPER

An experimental study of proton implantation in olivine

Thilo Bissbort[1,3,4] · Qinting Jiang[2] · Hans-Werner Becker[3] · Varvara Foteinou[3] · Sumit Chakraborty[1,3]

Abstract
Implantation of ions in minerals by high energy radiation is an important process in planetary and materials sciences. For example, the solar wind is a multi-ion flux that progressively modifies the composition and structure of near-surface domains in solar objects, like asteroids. A bombardment of a target by different elements like hydrogen (H) at various energies causes, among other things, the implantation of these particles in crystalline and amorphous materials. It is important to understand the mechanisms and features of this process (e.g., how much is implanted and retained), to constrain its contribution to the chemical budget of solar objects or for planning various material-science applications. Yet, there has been no detailed study on H implantation into olivine (e.g., the quantification of maximum retainable H), a major mineral in this context. We performed experiments on H implantation in San Carlos olivine at 10 and 20 keV with increasing fluences (up to 3×10^{18} at/cm^2). Nanoscale H profiles that result from implantation were analyzed using Nuclear Resonance Reaction Analysis after each implantation to observe the evolution of the H distribution as a function of fluence. We observed that after a systematic growth of the characteristic, approximately Gaussian shaped, H profiles with increasing fluences, a maximum concentration at H ~ 20 at% is attained. The maximum concentration is approximately independent of ion energy, but the maximum penetration depth is a function of beam energy and is greater at higher energies. The shapes of the profiles as well as the maximum concentrations deviate from those predicted by currently available models and point to the need for direct experimental measurements. We compared the depth profiles with predictions by SRIM. Based on observations from this study, we were able to constrain the maximum retainable H in olivine as a function of ion energy.

Keywords Hydrogen · Implantation · Olivine · Solar wind

Introduction

Modification of composition by implantation of ions in solid materials plays an important role in many planetary- and material-science applications. For example, any objects in the solar system are exposed to solar wind irradiation that progressively changes their structure and composition (Bennett et al. 2013). The solar wind consists of a variety of weathering-agents like electrons and different ions with energies that lie usually between few hundreds of eV to MeV, dependent on the solar activity (Bennett et al. 2013). This flux of charged particles constitutes a source for elements that are added to the compositional budget of solar objects by ion implantation. While some planets are protected from these charged particles by a surrounding atmosphere and magnetic field, atmosphere-less bodies like asteroids or the moon are affected by interaction between solar wind particles and their material. There are two major reasons why it is crucial to evaluate the process of ion implantation into solids, as it takes place in solar wind irradiation:

(i) Many solar objects are analyzed using remote sensing. Since the employed techniques probe primarily the surface-regions of objects, it is crucial to assess whether the upper layers are representative of the object's composition or if they were substantially modified by solar wind implantation (for example lunar regolith).

✉ Thilo Bissbort
thilo.bissbort@rub.de

1   Institute of Geology, Mineralogy, and Geophysics, Ruhr-University, Bochum, Germany

2   Department of Earth and Planetary Sciences, Yale University, New Haven, CT, USA

3   Central Unit for Ionbeams and Radionuclides RUBION, Ruhr-University, Bochum, Germany

4   Present Address: Department of Earth and Environmental Sciences, Ludwig-Maximilians-University, Munich, Germany

(ii) When dusts in the proto-solar disk are irradiated by the solar wind, their compositions will be modified, and consequently the composition of planets made from the dusts will also be modified by the solar wind. Recently studies on an asteroid (Itokawa; Daly et al. 2021) and meteorites (Chelyabinsk and Benenitra; Jin et al. 2021) suggested a role of the solar wind on the water (hydrogen) content in these materials and possible contribution of the solar wind as a source of water on Earth. There are several studies on the implantation of particles such as hydrogen in minerals (e.g., Lord 1968; Bibring et al. 1974; Schaible and Baragiola 2014), some key details such as the saturation level and the depth of penetration have not been well understood and characterized, particularly for olivine. Evaluating the role of ion implantation is therefore challenging because (a) while there are theoretical models (e.g., Tucker et al. 2019), it is difficult to make quantitative predictions a priori of how much H^+ (and other ions) would be implanted in a given material at different energy levels, (b) how robustly these ions, restricted to about 100 nm near the surface, would be retained, and (c) it is difficult to measure low concentration of H with high depth resolution in solids. Studies that combine experiments with calculated models, e.g., using a Binary Collision Approximation like *SDTrimSP* in Biber et al. (2020) or Molecular Dynamics simulations in Huang et al. (2022) further highlight the necessity for experimental work. In this work we address (a) and (c) through experiments in which San Carlos olivine crystals were implanted with hydrogen under controlled conditions. Subsequent analysis by Nuclear Resonance Reaction Analysis (NRRA) allowed us to observe the evolution of H implantation with increasing fluences at different ion energies. We point out that the interaction of solar wind with materials constitutes a complex interplay of many processes besides implantation (e.g., sputtering and irradiation by different types of particles) and target materials with different properties and structures (e.g., crystalline, and amorphous). Only a model that considers all these aspects can adequately describe the overall weathering of surfaces by solar wind and consequences for example for total retained H in solar objects. Thus, our study presents an important experimental step toward understanding the behavior and features of H implantation in San Carlos olivine, which can be incorporated in such future models.

The physics of accelerated ion–solid interaction

The energy loss of ions happens mainly by the interaction of ions with electrons of the material and to a smaller part by interaction with nuclei, the role of which increases toward smaller energies. Since the energy loss in each electronic interaction is very small, this process can be considered as quasi-continuous. The energy loss as a function of the penetration depth is described by the Bragg curve, which exhibits a peak at the end of the ion path. As a consequence, the ions have a defined range and since the process is statistical, the ion depth distribution could be expected to be a Gaussian one.

However, looking at experimental concentration depth profiles and from a more detailed theoretical perspective (Ziegler and Biersack 1985) it turns out that many implantation depth profiles are asymmetric. They can be calculated for example by Monte Carlo simulations (e.g., Ziegler et al. 2010) and are often described by e.g., a Pearson IV distribution (e.g., Wilson 1980; Ashworth et al. 1990; Lee and Park 2002; Zhang et al. 2008).

The shape of a concentration-depth profile is dependent on the ion's mass and energy and the chemical composition and density of the host material. For high fluences the general observation is that with increasing fluence the number of the implanted species retained in the host material increases but eventually reaches a saturation concentration. In this case, effects of defects produced by the implanted ions, changes in chemical composition of the host material, and the mobility of the implanted species become increasingly important. These features lead to a deviation of the depth profile shape at high fluences from the nearly symmetric Gaussian distribution at low fluences.

The energy of solar wind protons is a distribution of hundreds of eV to MeV. For example, an energy of 2 keV for H translates to an implantation range of up to ~25 nm in San Carlos olivine, which was calculated in a Monte Carlo simulation (SRIM, Ziegler et al. 2010). From the experimental point of view the measurement of the retained ions in such near surface regions is hampered by contaminations of the mineral's surface with hydrocarbons, which are present on almost all material surfaces handled in the lab environment or in standard high vacuum. These hydrogen-bearing substances can contribute to the determination of hydrogen when an integral method such as FTIR spectroscopy is used. Thus, a surface contamination can influence the quantification of implanted hydrogen when FTIR is used. Consequently, those measurements need to be performed in an UHV setup with the options of in situ surface cleaning, implantation, and analysis (Burke et al. 2011; Schaible and Baragiola 2014).

Several experimental studies have been performed to study H implantation in common planetary materials such as olivine. These range from the early work of Lord (1968) using chemical desorption to evaluate the hydrogen stored in the mineral after ion implantation to the recent work of Schaible and Baragiola (2014) who measured the implanted hydrogen with FTIR-spectroscopy. In this paper we present an alternative analytical route by measuring the implanted protons with Nuclear Resonance Reaction Analysis (NRRA). This technique allows to measure the hydrogen content as a function of depth with a depth resolution of some nanometers, thus

making a discrimination between surface contaminations and implanted hydrogen possible. Notably, the measured concentrations are independent of the chemical bonding of hydrogen (total H is measured) and the results are easy to quantify absolutely because reference standards are not needed. The reader is referred to Becker and Rogalla (2016) and Bissbort et al. (2021) for details on NRRA measurements in our facility.

For implantations at low energies, it becomes progressively difficult to determine the implantation fluence during implantation as well as the determination of the retained hydrogen in NRRA measurements. Therefore, we studied implantation profiles and the retention at proton impacting on olivine crystals with energies of 10 keV and 20 keV. Nanoscale hydrogen depth profiles that result from our experimental method are used to observe the development and behavior of hydrogen implantation with increasing fluences at different energies.

We propose a method to understand saturation behavior as a function of implantation energy based on our experiments. This in turn allows an extrapolation to lower energies that are relevant for the solar wind.

Experimental

We used samples of San Carlos olivine ($Mg_{1.81}Fe_{0.19}SiO_4$) to study the nature and the evolution of hydrogen distribution with depth that results from ion implantation as a function of beam energy, crystal orientation, and sample preparation. All but one sample were oriented and cut to obtain surfaces of about 4×4 mm, which were polished prior to irradiation. The olivine composition was determined using a *Cameca SX Five FE* electron microprobe in wavelength dispersive spectroscopy mode operated at 15 keV and 15nA. Standards used were San Carlos olivine (Mg), almandine (Al), fayalite (Si, Fe), diopside (Ca), and Ni-metal (Ni).

Two crystals—SC1 (010) and SC2 (010)—were implanted with hydrogen beams at energies of 20 keV and 10 keV, respectively, to study the effect of ion energies on the implantation behavior. Another sample SC3 (100) was tilted by 7° to the surface normal in a first series of implantation experiments (20 keV) to evaluate a possible effect of channeling during implantation. The channeling effect occurs when ion trajectories are aligned along atomic rows, usually with a critical angle $< 5°$ (Nastasi et al. 1996). This phenomenon might affect the implantation depth and the shape of the hydrogen concentration profile (e.g., broadening) (see Nastasi et al. 1996 for details on channeling). After this experimental series, sample

SC3 was re-ground, re-polished, and implanted without tilting, to provide a comparison between implantation in (100) to other orientations. Sample SC4 was implanted in (001) at 20 keV. Another sample, SCraw, was a natural San Carlos olivine crystal that was implanted at 20 keV without any prior preparation and a slightly convex surface to see how sample preparation might affect the outcome of implantation experiments. All samples were irradiated several times while H concentration profiles were obtained after each implantation using NRRA. Hereby, we were able to study the development of H contents and distributions with increasing fluences (Table 1).

The implantations were performed at the 100 kV implanter at the Central Unit for Ionbeams and Radionuclides (RUBION) at the Ruhr-University Bochum (Fig. 1). From the ion source the beam is analyzed by a 90-degree magnet. The beam then enters the implantation chamber through a collimator, which defines a circular implantation area of either 1 cm or 2 cm in diameter. The sample holder assembly is electrically insulated for the beam current measurement and a secondary suppression ring behind the entrance collimator at a voltage of -300 V prevents secondary electrons from falsifying the current measurements. During the implantation, the beam was scanned over the collimator to ensure a homogeneous implantation over the entire sample surface. The vacuum during the implantation was in the range of 10^{-6} mbar. The beam intensities were between 5 and 10 µA for 10 and 20 keV, respectively or fluxes of 2×10^{13} to 4×10^{13} at/cm²/s. To avoid charging up of the samples during the implantation they were embedded
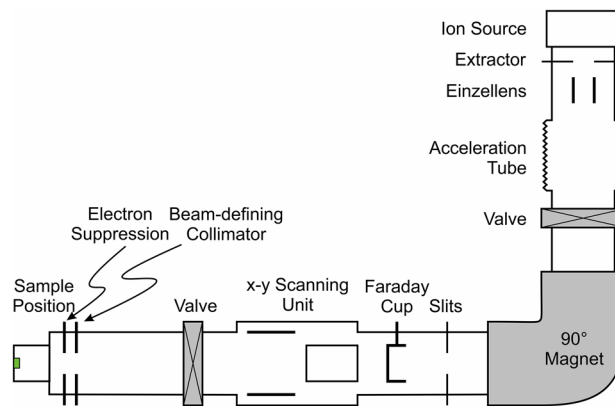
Fig. 1 Schematic layout of the implantation setup at the Ruhr-University Bochum (not to scale)

Table 1 San Carlos olivine samples used in this study

Sample	SC1	SC2	SC3	SC4	SCraw
Implanted surface	(010)	(010)	(100)	(001)	Close to (010)
Beam energy (keV)	20	10	20	20	20
Preparation	Polished	Polished	Polished	Polished	Natural surface
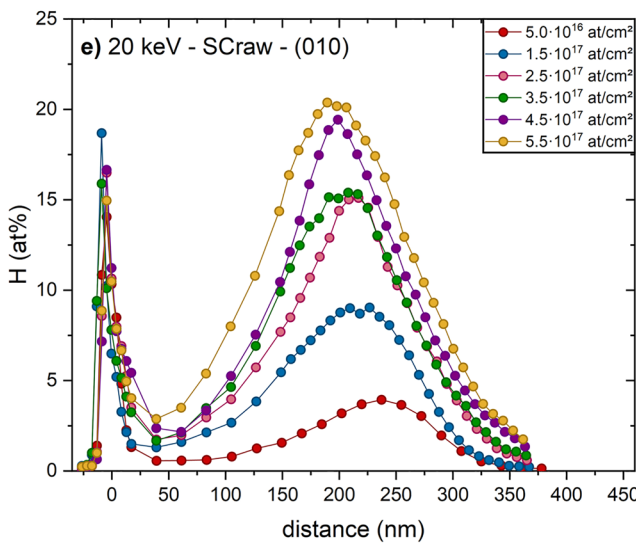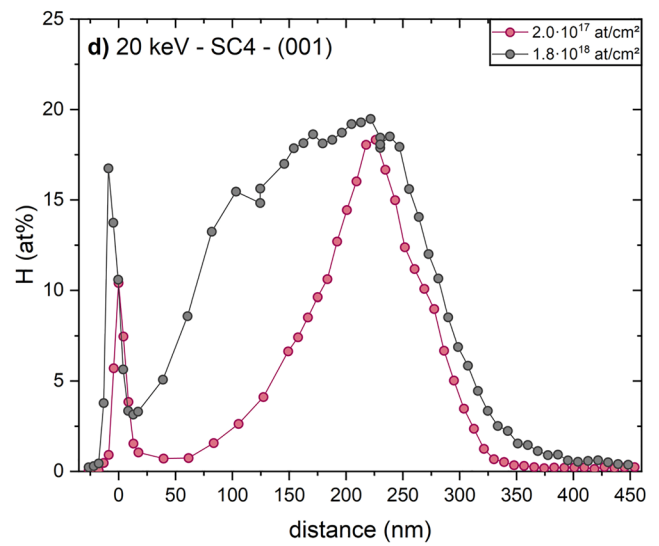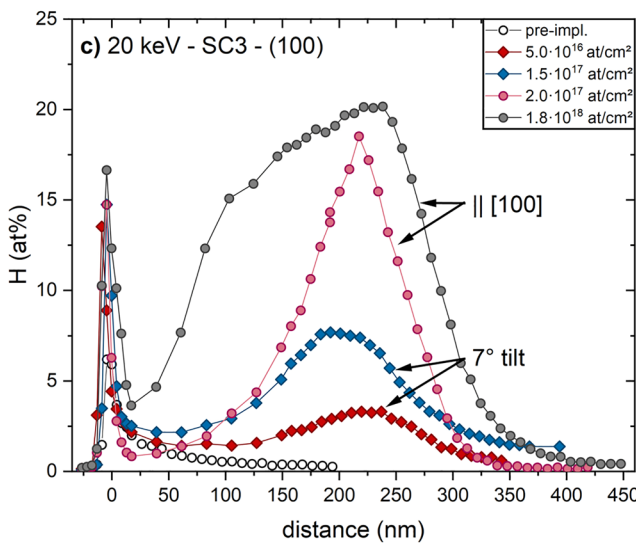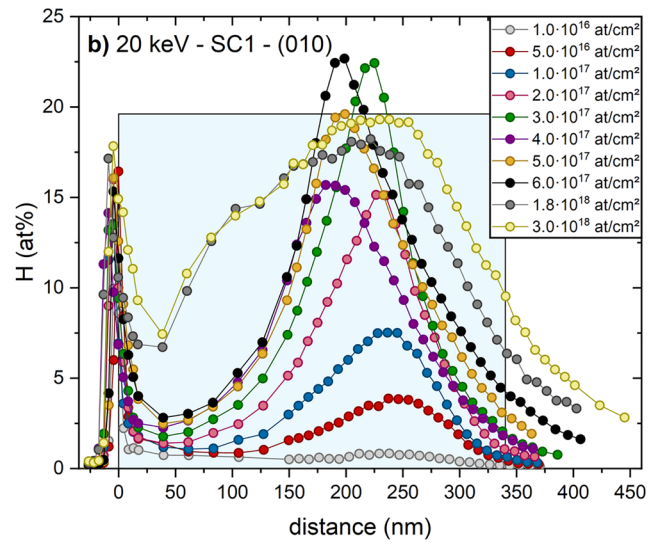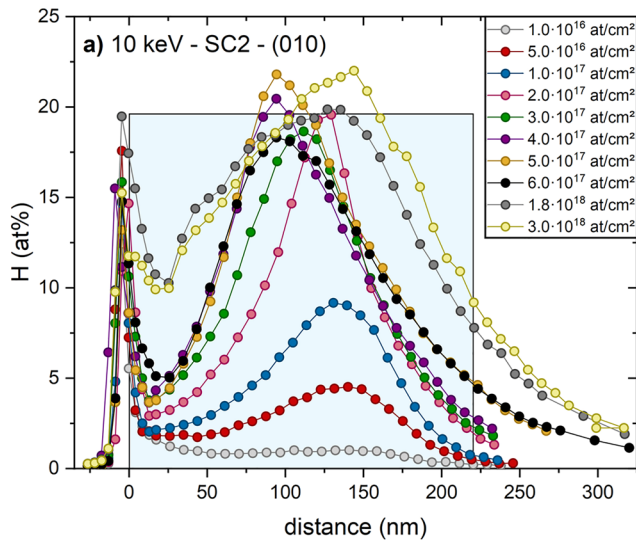
◄**Fig. 2** Hydrogen depth profiles for the five samples that were studied, showing the surface peak and the implantation profile for increasing implantation fluences. **a** Implantation at 10 keV in crystal surface (010). **b**–**d** Implantations at 20 keV in crystal surfaces (010), (100), and (001), respectively. **e** Implantation at 20 keV in a randomly oriented and unprepared surface. The marked areas (blue boxes) show an approximation of the maximum possible hydrogen loading attained at very high implantation fluences

in an aluminum foil which reached up to the surface leaving only the implantation spot open for implantation. The fluence could be determined by integrating the beam current with a commercial precision current integrator.

The depth profiles were measured after each implantation at the 4 MV Tandem accelerator at RUBION in Bochum. Details of the setup are described in Traeger et al. (2011). Briefly, NRRA utilizes the nuclear reaction $^{1}H(^{15}N,\alpha\gamma)^{12}C$ with a resonance at a beam energy of 6.4 MeV (Lanford 1992; Becker and Rogalla 2016; Wilde and Fukutani 2014). The ^{15}N beam from the accelerator is focused by two collimators to a beam spot of 1.5 mm diameter. The sample is placed at the end of a pipe, reaching into the center of a 4×4-inch NaI borehole detector, which has a 44% detection efficiency for the 4.4 MeV γ-rays that are a product of the nuclear reaction. The sample assembly is designed as a good Faraday cup for beam current measurements and equipped as well with a secondary electron suppression at 300 V. During the measurement with typically 40 nA beam current, the vacuum was in the range of 10^{-8} mbar. Increasing the beam energy above 6.4 MeV leads to a shift of the nuclear reaction toward greater depths in the sample, as the ^{15}N energy must be reduced by ion-material interaction for the reaction to occur at the resonance energy. Finally, analysis of H concentrations at incrementally increased ion energies (e.g., by 20 keV steps) constitutes a H depth profile. Several test measurements showed that the samples did not deteriorate, and no loss of hydrogen could be observed from the analyzing beam. The samples were mounted with an aluminum foil in the same fashion as for the implantation.

Results and discussion

The measured raw data, which are the γ-yields from the nuclear reaction as a function of the beam energy, can be converted into a hydrogen concentration as a function of depth in the sample using the stopping cross section of ^{15}N-ions in olivine and hydrogen from SRIM (Ziegler et al. 2010) at 6.4 MeV (238 eV/(10^{15} at/cm²) and 60.9 eV/ (10^{15} at/cm²), respectively) for the calculation of the hydrogen concentration. The stopping power to determine the depth scale was calculated with a density of 3.32 g/cm³ to e.g., 2.27 keV/nm and 2.38 keV/nm for anhydrous SC olivine and SC olivine with 20 at% H, respectively. This conversion has to be done successively from the surface to the depth, calculating a stopping power for each depth according to the hydrogen concentration at that depth. The results are shown in (Fig. 2).

The surface peaks that result from adsorption of hydrocarbons on the sample surfaces can be seen clearly in all cases, and they are well separated from the implantation profiles. The implantation profiles exhibit an asymmetric shape with a tail to the surface. At low fluences the maxima of the peak are at a depth of ~ 120 nm and ~ 210 nm, for the 10 and 20 keV implantations in SC2 and SC1, respectively. This is significantly higher than the depth calculated from SRIM (Fig. 3) which is not surprising since the stopping power values for low energy protons are not very accurately known and the available data deviate substantially from each other (Ziegler et al. 2010). This highlights the need for direct experimental measurements.

There is a systematic development of the observed implantation profiles with increasing fluences that can be subdivided into two stages. (i) At low fluences the concentration maximum (peak) systematically growths with increasing fluences. (ii) This systematic increase in the maximum concentration is not observed at high fluences. Instead, at some threshold in fluence (e.g., 3.0×10^{17} at/ cm² in SC1) a maximum in concentration is attained that is not exceeded in subsequent implantations. Instead, the maxima of the concentration peaks vary within a limited concentration range around ~ 20 at% H at fluences above the thresholds. This results in an "oscillation" of the peak. The described features are observed in 10 keV and 20 keV experiments, which implies that this behavior, except for the depth of implantation, is independent of implantation energies. Also, the overall implantation profiles become progressively broader with increasing fluences. Likewise, the maxima appear to shift for medium fluences slightly toward lower depths and reach, for very high fluences, the value of the low fluence implantation again (Fig. 2). The origin of these variations is unclear, and we attribute this to local phase transitions at high fluences caused possibly by amorphization and recrystallisation effects and/or chemical changes at certain depths of the samples. These aspects require further detailed studies coupled with microstructural characterization of the samples.

Implantation experiments in sample SC3 (100) at 20 keV with its surface tilted by 7° during implantation followed by implantations in the same sample (but re-polished) without tilt [parallel to (100)] reveal that channeling does neither significantly affect the depth of implantation nor the shape of the concentration profiles. Also, channeling does not cause the observed difference between the observed implantation depth and that predicted by SRIM (Fig. 3). A comparison between all oriented samples (SC1, SC3, and SC4) at 20 keV proves that the penetration depth and the maximum
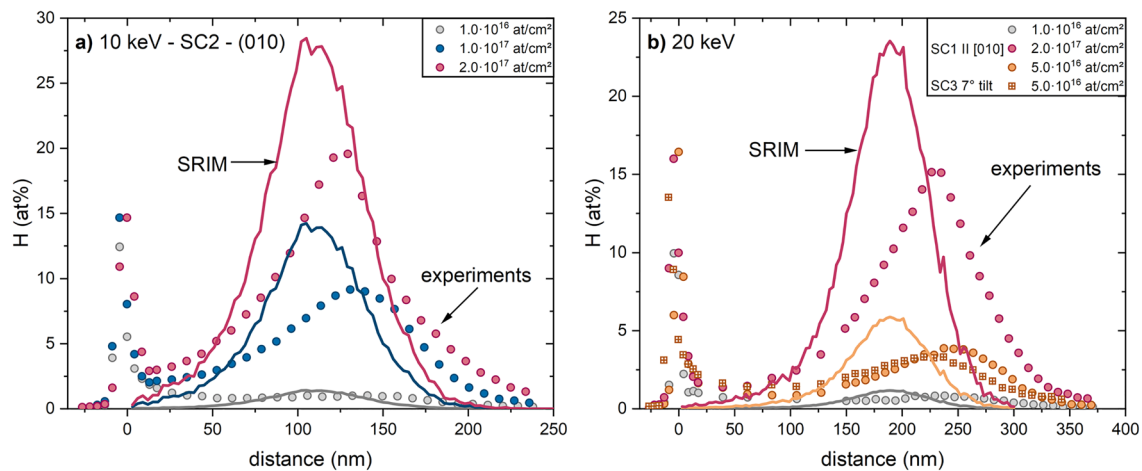
Fig. 3 Comparison between calculated H depth profiles using SRIM (solid lines) and H depth profiles obtained from implantation experiments (filled circles) at different fluences and two energies, 10 keV (**a**) and 20 keV (**b**). Simulated profiles do not agree with the measured ones in terms of peak locations, widths of the peaks, and maximum concentrations, especially at higher fluences. The displacement of the experimental profiles toward greater depth implies that the real stopping power of H in olivine is smaller than that predicted by SRIM and the differences in peak widths indicate greater energy straggling in experiments. A comparison in **b** between implantation in sample SC1 along [010] (orange circles) and in sample SC3 that was tilted by 7° to [100] to prevent channeling effects shows only minor differences and does not explain the discrepancy to the SRIM profile (orange solid line). These aspects and the absence of any saturation effect in SRIM profiles highlights the need to perform experiments
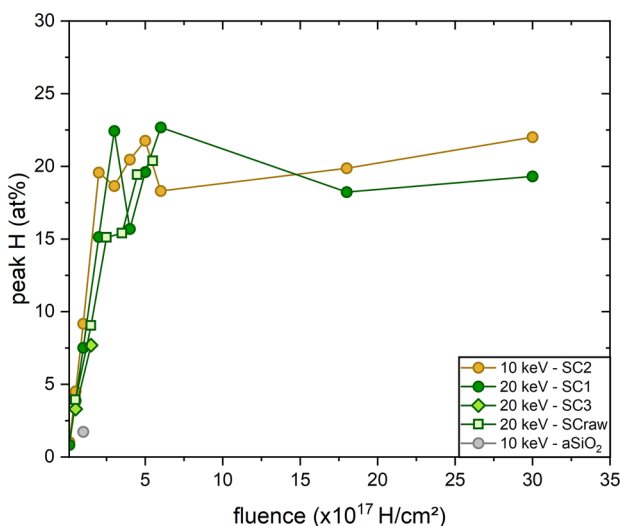

Fig. 4 Maximum of the implantation profiles from Fig. 2 excluding the surface peak, for increasing implantation fluences. The maximum of an implantation into an amorphous SiO_2 layer is also indicated (see Fig. 6 and text)

concentration (profile peak) is unaffected by the orientation of the crystals.

In Fig. 4 the peak heights of the implantation profiles for the 10 keV as well as the 20 keV implantations are plotted against the implantation fluence. Regardless of the features discussed above, the general behavior is that with increasing fluence the maximum of the implantation profile first increases and eventually reaches a saturation value at about 19.6 ± 1.6 at%. Notably, this local saturation, which is the maximum attainable concentration, is similar for both implantation energies. Therefore, we conclude that saturation effects in the retention of protons in olivine is governed by a maximum local concentration that can be attained over the entire investigated depth of the sample with increasing fluences. With increasing fluences, higher amounts of retained hydrogen in the olivine are achieved slowly by filling up the volume below the maximum range toward the surface until the maximal possible local concentration is reached. This behavior is clearly seen in the data of high implantation fluences in Fig. 2.

To determine the total hydrogen retained in the samples, the implantation profiles were integrated with depth excluding the surface peak (which, as noted above, results from H adsorbed *on* the surface of crystals from contamination, and not those implanted in the crystal). This integration can be done directly with the raw data and the total γ-yield (which is an absolute measure of the H content) integrated over the beam energies gives the total hydrogen content, independent of the assumed / calculated stopping power (Becker and Rogalla 2016). The width of the integrated area was calculated from the energy difference between start and end of the profiles and the stopping cross section of dry olivine. This precludes the necessity to know the density. Figure 5 shows the results of this integration as a function of the fluence. Total amounts of hydrogen in the samples that were determined by integrating the profiles increase linearly with
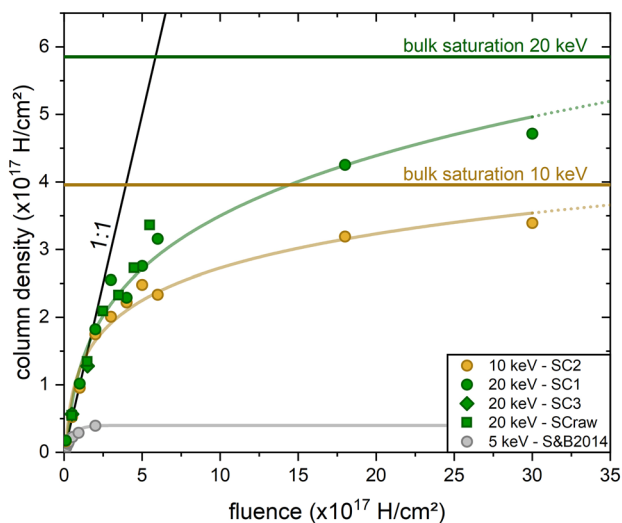
Fig. 5 Column densities measured for increasing implantation fluences and implantation energies of 10 (yellow) and 20 keV (green). Data from Schaible and Baragiola (2014) with an implantation energy of 5 keV are given for comparison (gray). The solid black line indicates the case when all implanted ions would be retained in the sample

increasing fluences in the low-fluence domain ($< 2 \times 10^{17}$ at/cm^2) and almost all implanted hydrogen is retained. The trend deviates from complete retention for higher fluences ($\geq 2 \times 10^{17}$ at/cm^2). Instead, retention of implanted hydrogen becomes less efficient with increasing fluences. This makes a direct observation of a complete bulk saturation in experiments (i.e., the entire volume between implantation depth and surface is loaded with hydrogen at the local saturation level; see horizontal lines Fig. 5) impossible. However, the difference in bulk saturation values for different implantation energies in olivine appear to be caused solely by the larger volumes available with increasing implantation energies between surface and the range of the protons. Significant diffusion to depths larger than the range of ions during implantation is not observed in olivine. Based on these observations we estimated the maximum attainable amount of hydrogen in San Carlos olivine as function of ion energy (blue boxes in Fig. 2, solid horizontal lines "bulk saturation" in Fig. 5). We may define an effective depth, as the depth where the falling tail of the implantation curve reaches the 50% point (see rectangular boxes in Fig. 2). This effective depth is 220 nm and 340 nm, for the 10 keV and 20 keV implantations, respectively. We note here that the cut-off at the 50% point i.e., at half-maximum is set arbitrarily and an alternate choice (e.g., 90% fall-off from the maximum value, closer to the tail of the curve) would lead to different numerical values in the subsequent discussion; but the physical behavior that is discussed would remain the same. Combined with the values of 19.6 ± 1.6 at% for the maximum local

concentration the cut-off at 50% fall-off leads to a maximum column density (i.e., bulk saturation) of $4.0 \pm 0.3 \cdot 10^{17}$ and $5.9 \pm 0.5 \cdot 10^{17}$ at/cm^2 for 10 keV and 20 keV, respectively. Retained amounts of hydrogen approach these bulk saturation values asymptotically toward high fluences. Fits to our data are meant to guide the eye (2nd order power-law, solid curves in Fig. 5) and have no physical meaning. However, it is noteworthy that the equation used by Schaible and Baragiola (2014) attains a constant column density value with high fluences, whereas our experiments clearly indicate that bulk saturation is not attained yet at these fluences. Hence, their equation is unsuitable to fit our data. An adequate equation must fulfill following requirements: (i) The total amount of hydrogen must be zero at a fluence of zero. (ii) An increase in retained hydrogen with fluence must follow a linear trend with almost ideal retention up to some threshold in fluence. (iii) Above this threshold the retained hydrogen asymptotically approaches a bulk saturation that must not be exceeded. We note that requirement (iii) is related to the assumption that the available volume between penetration depth and surface is completely loaded with H at high fluences and no more H can be added. The details of the column density-fluence relation are discussed in a separate paper in connection to the application to water acquisition in the proto-planetary disk. The saturation is obtained at lower fluences for the 10 keV implantation, as the volume that can be filled by implantation is smaller due to the lower penetration depth at lower energies. The values reported by Schaible and Baragiola (2014) at 5 keV are also given in the figure with a saturation column density at $0.4 \cdot 10^{17}$ at/cm^2.
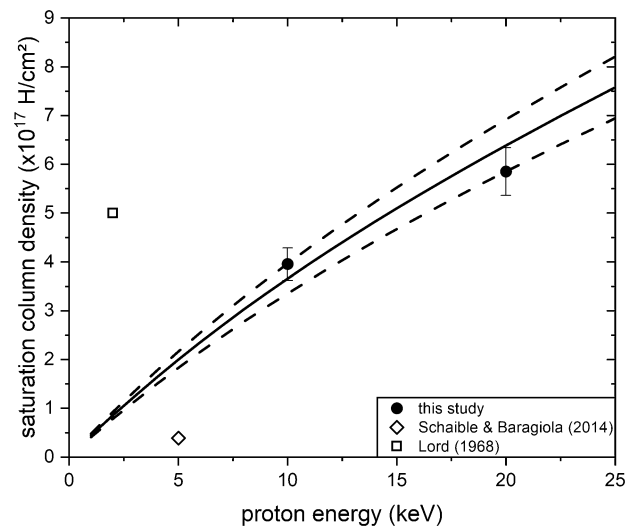
To compare our measurements employing NRRA with FTIR measurements of Schaible and Baragiola (2014) we implanted protons of 10 keV into a well-defined layer—namely, an amorphous electronic grade SiO_2 layer of 300 nm thickness grown by dry thermal oxidation of a silicon wafer (Siegert Wafer GmbH, Germany). Like in the work of Schaible and Baragiola (2014), the implantation was done with a fluence of 1×10^{17} at/cm^2, which is far above the saturation level. Figure 6 shows the hydrogen depth profile of the layer before and after the implantation. The characteristics of the profiles are completely different from those in olivine—no Gaussian shaped profile is recognizable, and the entire layer is homogeneously loaded with a mean hydrogen concentration of 1.71 ± 0.11 at% of H. The nominal thickness of the amorphous layer is very well reproduced by the measurement, i.e., the analyzed hydrogen depth profile is 300 nm long. In this case the total hydrogen retained in the layer is dependent on the thickness of the layer, which was 300 nm in our case. The column density that is obtained by integrating the area is 3.71 ± 0.24 at/cm^2. The column density denotes the hydrogen concentration in the sample integrated over the entire depth (unit = at/cm^2) in contrast to the concentrations given at a given depth (unit = at/cm^3). The layer
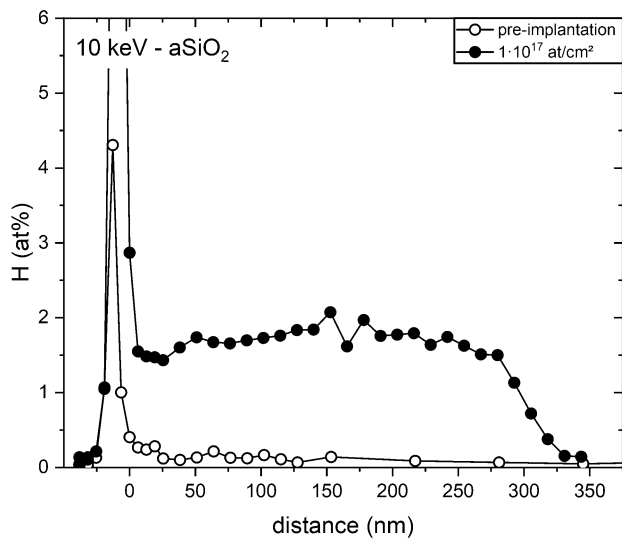
Fig. 6 Hydrogen depth profile of an amorphous SiO_2 layer of 300 nm nominal thickness implanted with 1×10^{17} at/cm^2. The open circles show the hydrogen profile of the layer before the implantation. Note the difference in shape of this profile in comparison to those for olivine, see text for details

Fig. 7 Raw estimation for the saturation of hydrogen implantation in olivine as a function of the implantation energy. The results of previous work are also given (see text). The dashed lines indicate the uncertainties based on the error of the determination of the saturation peaks in Fig. 2

implanted in the work of Schaible and Baragiola (2014) had a thickness of 200 nm and a column density of 2.4 ± 0.3 at/cm^2 (estimated from their Fig. 4). Our value scaled to 200 nm would be 2.47 ± 0.16 at/cm^2, which is in excellent agreement with the results of Schaible and Baragiola (2014). The difference in the outcome of H implantation between olivine and an amorphous SiO_2 film also highlights how the implantation behavior depends on the nature of the material being implanted.

For an extrapolation of the maximum column density toward lower energies the ranges of protons at lower energies are needed, as our experimental results indicate that the amount of retainable H is controlled by the available volume between surface and penetration depth. Since the ranges given by SRIM do not agree with our measured values, we use our values for the effective depth and use these with the energy dependence of ranges given by SRIM. The resulting total column densities are given in Fig. 7 as a solid line, with upper and lower limits shown as dashed lines showing the limits of uncertainty of our measurements. The results of Lord (1968) and Schaible and Baragiola (2014) for implantation in olivine are also shown for comparison. The value of Lord (1968) is substantially higher while the result of Schaible and Baragiola (2014) is somewhat lower. The difference of our results from the early data of Lord (1968) might be due to the experimental difficulties connected with the desorption measurements. Notably, a desorption experiment cannot distinguish between the implanted H and the H adsorbed

on the surfaces of crystals, and the additional adsorbed H would cause the results to deviate in the right direction i.e., higher than the values measured by us (where adsorbed H could be excluded, see above). When comparing our results to the results of Schaible and Baragiola (2014) one has to keep in mind that FTIR measurements determine the hydrogen bound in OH groups only while the NRRA techniques measures the total hydrogen content independent of the nature of chemical binding (e.g., (OH), H, H_2 etc. are all "seen" by the technique). Again, this may explain the direction of deviation of the results (lower) from ours (see also a separate paper Jiang et al., in prep.).

Our depth profiles of implanted hydrogen in olivine as a function of fluence reflect how hydrogen concentrations in planetary materials, like olivine, may evolve during solar wind irradiation. Hydrogen penetrates to a certain depth and accumulates at this depth until the saturation level is reached. Although, the penetration depth of hydrogen is only tens to hundreds of nanometers, the saturation level of hydrogen found in this study (several wt% in olivine) far exceeds the hydrogen solubility in olivine coexisting with water under the same condition (~ 10^{-18} wt% at 300 K, extrapolated from Zhao et al. 2004). For micrometer-sized dusts in the protoplanetary disk, one could expect a large mass fraction of hydrogen. To evaluate the solar wind contribution in more detail, more factors like dust size, exposure time to solar wind, disk structure need to be considered. Also, further experiments to study the potential

role of amorphization affecting the saturation are expected in the future.

Summary and conclusion

The implantation profiles of protons in olivine implanted with ion beams of 10 keV and 20 keV have been studied with the Nuclear Resonance Reaction Analysis. We found that the saturation in the retention of implanted ions is due to a maximum local concentration of hydrogen in olivine by implantation. This local saturation is independent of beam energies. Thus, the total amount of hydrogen that can be retained in San Carlos olivine is a function of the proton range, which is greater for higher ion energies. We measured the saturation column density for implantation energies of 10 and 20 keV to be $4.0 \pm 0.3 \cdot 10^{17}$ and $5.9 \pm 0.5 \cdot 10^{17}$ at/cm^2 respectively (subject to certain assumptions, as outlined above). An approximate functional form to extrapolate these results toward lower energies that may be relevant for calculations involving solar winds is presented. Solar wind irradiation could be a possible source for the hydrogen of terrestrial planets.

Declarations

Conflict of interest The authors have no competing interests to declare that are relevant to the content of this article.

References

Ashworth DG, Oven R, Mundin B (1990) Representation of ion implantation profiles by Pearson frequency distribution curves. J Phys D Appl Phys 23(7):870–876. https://doi.org/10.1088/0022-3727/23/7/018

Becker HW, Rogalla D (2016) Nuclear Reaction Analysis. In: Fritzsche H, Huot J, Fruchart D (eds) Neutron scattering and other nuclear techniques for hydrogen in materials. Springer, Cham, pp 315–336

Bennett CJ, Pirim C, Orlando TM (2013) Space-weathering of solar system bodies: a laboratory perspective. Chem Rev 113(12):9086–9150. https://doi.org/10.1021/cr400153k

Biber H, Szabo PS, Jäggi N, Wallner M, Stadlmayr R, Moro MV et al (2020) Solar wind helium ion interaction with Mg and Fe rich pyroxene as mercury surface analogue. Nucl Instrum Methods Phys Res Sect B 480:10–15. https://doi.org/10.1016/j.nimb.2020.07.021

Bibring JP, Langevin Y, Maurette M, Meunier R, Jouffrey B, Jouret C (1974) Ion implantation effects in "cosmic" dust grains. Earth Planet Sci Lett 22(3):205–214. https://doi.org/10.1016/0012-821X(74)90083-1

Bissbort T, Becker HW, Fanara S, Chakraborty S (2021) Novel approach to study diffusion of hydrogen bearing species in silicate glasses at low temperatures. Chem Geol 562:120037. https://doi.org/10.1016/j.chemgeo.2020.120037

Burke DJ, Dukes CA, Kim JH, Shi J, Famá M, Baragiola RA (2011) Solar wind contribution to surficial lunar water: Laboratory investigations. Icarus 211(2):1082–1088. https://doi.org/10.1016/j.icarus.2010.11.007

Daly L, Lee MR, Hallis LJ, Ishii HA, Bradley JP, Bland PA et al (2021) Solar wind contributions to Earth's oceans. Nat Astron. https://doi.org/10.1038/s41550-021-01487-w

Huang Z, Nomura KI, Morrissey LS, Wang J (2022) Molecular dynamics simulation of solar wind implantation in the permanently shadowed regions on the lunar surface. Geophys Res Lett 49:18. https://doi.org/10.1029/2022GL099333

Jin Z, Bose M, Lichtenberg T, Mulders GD (2021) New Evidence for wet accretion of inner solar system planetesimals from meteorites chelyabinsk and benenitra. Planet Sci J 2(6):244. https://doi.org/10.3847/PSJ/ac3d86

Lanford WA (1992) Analysis for hydrogen by nuclear reaction and energy recoil detection. Nucl Instrum Methods Phys Res Sect B: Beam Interact Mater Atoms 66(1–2):65–82. https://doi.org/10.1016/0168-583X(92)96142-L

Lee S, Park S (2002) Empirical depth profile model for ion implantation in 4H-SiC. J Korean Phys Soc 5:591–593

Lord HC (1968) Hydrogen and helium ion implantation into olivine and enstatite: retention coefficients, saturation concentrations, and temperature-release profiles. J Geophys Res 73(16):5271–5280. https://doi.org/10.1029/JB073i016p05271

Nastasi M, Mayer JW, Hirvonen JK (1996) Ion-solid interactions. Fundamentals and applications, 1st edn. Cambridge: Cambridge Univ. Press (Cambridge solid state science series). Online

verfügbar unter https://www.cambridge.org/core/books/ionsolid-interactions/1E0F510F4813027285B6D2681104DF89

Schaible MJ, Baragiola RA (2014) Hydrogen implantation in silicates: the role of solar wind in SiOH bond formation on the surfaces of airless bodies in space. J Geophys Res Planets 119(9):2017–2028. https://doi.org/10.1002/2014JE004650

Traeger F, Kauer M, Wöll CH, Rogalla D, Becker HW (2011) Analysis of surface, subsurface, and bulk hydrogen in ZnO using nuclear reaction analysis. Phys Rev B 84(7):75462. https://doi.org/10.1103/PhysRevB.84.075462

Tucker OJ, Farrell WM, Killen RM, Hurley DM (2019) Solar wind implantation into the lunar Regolith: Monte Carlo simulations of H retention in a surface with defects and the H 2 exosphere. J Geophys Res Planet 124(2):278–293. https://doi.org/10.1029/2018JE005805

Wilde M, Fukutani K (2014) Hydrogen detection near surfaces and shallow interfaces with resonant nuclear reaction analysis. Surf Sci Rep 69(4):196–295. https://doi.org/10.1016/j.surfrep.2014.08.002

Wilson RG (1980) The pearson IV distribution and its application to ion implanted depth profiles. Radiat Effects 46(3–4):141–147. https://doi.org/10.1080/00337578008209163

Zhang H, Gao M, Xu L, Lin M, Niu X, Lv W (2008) United Gauss–Pearson-IV distribution model of ions implanted into silicon. Solid State Ion 179(21–26):832–836. https://doi.org/10.1016/j.ssi.2008.01.084

Zhao YH, Ginsberg SB, Kohlstedt DL (2004) Solubility of hydrogen in olivine: dependence on temperature and iron content. Contrib Mineral Petrol 147(2):155–161. https://doi.org/10.1007/s00410-003-0524-4

Ziegler JF, Biersack JP (1985) The stopping and range of ions in matter. In: Bromley DA (ed) Treatise on heavy-ion science: astrophysics, chemistry, and condensed matter, vol 6. Springer, Boston, pp 93–129

Ziegler JF, Ziegler MD, Biersack JP (2010) SRIM—the stopping and range of ions in matter (2010). Nucl Instrum Methods Phys Res Sect B Beam Interact Mater Atoms 268(11–12):1818–1823. DOI: https://doi.org/10.1016/j.nimb.2010.02.091. www.srim.org